

Fluid–structure interaction modelling of nonlinear aeroelastic structures using the finite element corotational theory

A. Relvas^a, A. Suleman^{b,*}

^a*Department of Mechanical Engineering, IDMEC-Instituto Superior Técnico, Av. Rovisco Pais, 1049 - 001 Lisbon, Portugal*

^b*Mechanical Engineering Department, University of Victoria, P.O. Box 3055, Victoria, B.C., Canada*

Received 7 February 2005; accepted 2 September 2005
Available online 9 November 2005

Abstract

The application of the finite element corotational theory to model geometric nonlinear structures within a fluid–structure interaction procedure is proposed. A dynamic corotational approximately-energy-conserving algorithm is used to solve the nonlinear structural response and it is shown that this algorithm's application with a four-node flat finite element is more stable than the nonlinear implicit Newmark method. This structural dynamic algorithm is coupled with the unsteady vortex-ring method using a staggered technique. These procedures were used to obtain aeroelastic results of a nonlinear plate-type wing subjected to low speed airflow. It is shown that stable and accurate numerical solutions are obtained using the proposed fluid–structure interaction algorithm. Furthermore, it is illustrated that geometric nonlinearities lead to limit cycle oscillations.

© 2005 Elsevier Ltd. All rights reserved.

Keywords: Nonlinear; Aeroelasticity; Corotational; Fluid–structure interaction

1. Introduction

Fluid–structure interaction (FSI) problems are characterized by the coupling between the fluid and the structure. One important application field is aeroelasticity.

Most of the work on nonlinear aeroelasticity reported in the open literature has concentrated on improving the modelling of the fluid flow using the nonlinear Euler/Navier–Stokes equations (Liu et al., 2001, 2000; Lee-Raush and Batina, 1993; Alonso et al., 1995; Alonso and Jameson, 1994).

More recently, there is an increased interest in new aircraft design with high aspect-ratio wings, which are very flexible and consequently structural geometric nonlinear effects play an important role in the system dynamics. Some of the pioneering developments considering nonlinear structures in aeroelasticity were reported by Dowell. He studied limit cycle oscillations (LCO) of plates (Dowell, 1966, 1967) and curved plates (Dowell, 1969, 1970). More recently, Weiliang and Dowell (1991) studied for the first time LCO of a cantilever plate in a supersonic flow. The plate was modelled using the von Kármán theory and the Rayleigh–Ritz approach was used to solve the nonlinear oscillations. The fluid was modelled using the quasi-steady supersonic aerodynamic theory. This paper studied the effect of the length to width ratio on vibration. Tang et al. (1998) studied nonlinear aeroelastic systems using a reduced-order

*Corresponding author. Tel.: +1 250 721 6039.

E-mail addresses: anarelvas@ist.utl.pt (A. Relvas), suleman@uvic.ca, suleman@ist.utl.pt (A. Suleman).

aerodynamic model. They studied an airfoil with a trailing-edge flap, including structural free-play nonlinearities, and compared it with experimental results. Tang et al. (1999b) also studied LCO in low-aspect delta wing models in low subsonic flow. A vortex lattice aerodynamic model was used and the structure was modelled using Lagrange equations based on the von Kármán's plate equations. A cantilevered wing LCO in low subsonic flow was also studied (Tang et al., 1999a) using the mentioned theories. Patil and Hodges (1998), Patil et al. (2001), and Patil (1999) have studied high aspect ratio wings with structural nonlinearities using a geometrically-exact mixed formulation for dynamics of moving beams (Hodges, 1990; Patil et al., 1998). The fluid was modelled with finite-state unsteady aerodynamics with the ability to model dynamic stall. The effects of the geometric nonlinearities on the aeroelastic behaviour were also studied by Patil et al. (1999). It was shown that curved beams and straight wings behave differently due to the curved beams being affected by the curvature-induced changes in the effective bending-torsion coupling and by the direction of the aerodynamic loading. Garcia and Guruswamy (1999) applied a coupled nonlinear beam finite element theory with an existing Navier–Stokes aerodynamic model. They studied static aeroelasticity of three high aspect ratio wings in the transonic regime. Kamakoti et al. (2002) presented a summary of recent aeroelastic models.

Although there is some research being done in the field of nonlinear aeroelastic structures, it is essential to improve the modelling of the structural field within existent fluid–structure interaction methods. The method proposed in this article can be applied within an existent linear fluid–structure interaction software and a nonlinear fluid–structure interaction solution can be obtained.

Staggered algorithms are very popular to solve these problems. The structure and fluid solutions are determined separately and each treats the interaction effects as external disturbances. This procedure allows the use of existing software developed in the structural and fluid dynamics fields and takes advantage of the research developments that have been made in both fields. Some of the first publications on applying staggered algorithms to solve fluid–structure interaction problems were done by Felippa and Park (1980), Park and Felippa (1980), and Park et al. (1977). They studied these algorithms' stability and accuracy. Piperno et al. (1995) studied the partitioned procedures for the transient solution of coupled aeroelastic problems. The accuracy, stability, heterogeneous computing, sub-cycling, and parallel processing were analysed. It has been shown (Farhat and Lesoinne, 1998, 2000) that the “Improved Serial Staggered” (ISS) algorithm is more stable, accurate, and efficient than the conventional staggered algorithms. In the present article the ISS algorithm proposed by Farhat and Lesoinne (1998, 2000) is used.

In the present study, it is proposed to use the finite element corotational theory to solve the geometric nonlinear structure. This theory separates the rigid body motion out of the description of strains.

The theory presented in the present article is based on the work by Crisfield, who developed a “consistent corotational formulation” (Crisfield, 1990) and applied it to three-dimensional beams. The corotational theory application (Peng and Crisfield, 1992) to triangular shell elements with constant strain and constant curvature was also documented. Later (Crisfield et al., 1995), a lower-order element for elastic and elasto-plastic large-strain elements was developed. A three-dimensional theory (Moita and Crisfield, 1996) with an extension to large-strain formulation and with emphasis on hyperelasticity was developed and applied to an eight-node brick element with three translational degrees of freedom. A unified corotational framework (Crisfield and Moita, 1996) for solids, shells, and beams was also presented and it was applied to triangular and quadrilateral shell elements with rotational degrees of freedom, to facet shell elements based on Morley's triangle, and to three-dimensional beams. A static corotational simple faceted shell element was presented (Crisfield et al., 1997) and nonlinear energy conserving dynamics techniques were developed.

Furthermore, the nonlinear implicit dynamic algorithms are often unstable. To overcome that, an implicit dynamic corotational method that approximately conserves the energy was proposed by Crisfield and Shi (1994). This theory (“energy conserving” or “approximately energy conserving”) was applied to beams (Crisfield et al., 1996). In the present article, this dynamic implicit procedure is applied to a four-node flat element. The corotational theory has the advantage of making possible to use already developed linear codes to obtain the nonlinear solution.

The corotational theory developed by Rankin and Brogan (1986) was used to study an unrestrained and flexible aircraft during high-G maneuvers by Farhat et al. (2001). In that study, the large rigid body motions of the aircraft were considered and the structure presented small deformations, whereas the present article considers large structural deformations.

In short, this article presents the nonlinear corotational theory application with a four-node flat element. A corotational nonlinear dynamic implicit algorithm that conserves the energy approximately is also used. Two structural problems are solved to show the accuracy and stability properties of this algorithm. To indicate the superiority of the presented method, the same problems are also solved using the nonlinear implicit Newmark method. Then, the improved serial staggered fluid–structure interaction algorithm is used to couple the corotational structural theory presented and the unsteady vortex-ring method. A nonlinear clamped plate subjected to low speed airflow is studied to illustrate the fluid–structure interaction procedure.

2. Geometrically nonlinear structural model

In what follows, the general idea of the corotational theory is delineated. For more detail, see Moita and Crisfield (1996), Crisfield and Moita (1996), Crisfield et al. (1996), Moita (1994), Crisfield (1997), and Relvas (2002).

2.1. The corotational theory

In the finite element corotational description, one element displacement is considered to be composed of a rigid body motion of the base configuration and of the corotated element deformations (Fig. 1). Each element has a local coordinate system X_L, Y_L, Z_L attached to a node and this system continuously rotates with the element. The linear formulation is valid with respect to this system. The coordinate system rotation produces the nonlinearity. In this article a four-node flat element is used with five degrees of freedom per node \mathbf{p} (three translations \mathbf{d} and two rotations θ) based on Mindlin’s assumptions.

Consider a generic element k transformation matrix \mathbf{T}_k , which relates a small change of the nodal displacement vector $\delta \mathbf{p}_{Lk}$ in the local coordinate system, and nodal displacement vector $\delta \mathbf{p}_k$ in the global coordinate system (see the two-dimensional diagram in Fig. 1, considering only the translational degrees of freedom \mathbf{d}). This can be written as

$$\delta \mathbf{p}_{Lk} = \mathbf{T}_k \delta \mathbf{p}_k. \tag{1}$$

As the virtual work in the local system is equal to the virtual work in the global system ($\delta \mathbf{p}_{Lk}^T \mathbf{f}_{iLk} = \delta \mathbf{p}_k^T \mathbf{f}_{ik}$), the global internal nodal forces \mathbf{f}_{ik} and the local internal forces \mathbf{f}_{iLk} are related as

$$\mathbf{f}_{ik} = \mathbf{T}_k^T \mathbf{f}_{iLk}. \tag{2}$$

Differentiating Eq. (2) and defining \mathbf{K}_{Ik} as the k th element linear stiffness matrix and, recalling that $\mathbf{f}_{iLk} = \mathbf{K}_{Ik} \mathbf{p}_{Lk}$ is valid because the linear relationship is verified at the local level, one obtains the k th element nonlinear tangent stiffness matrix \mathbf{K}_{Tk} :

$$\mathbf{K}_{Tk} = \mathbf{T}_k^T \mathbf{K}_{Ik} \mathbf{T}_k + \mathbf{K}_{\tau\sigma k}. \tag{3}$$

The matrix $\mathbf{K}_{\tau\sigma k}$ is related with the small variation of \mathbf{T}_k and can be explicitly determined. The matrix \mathbf{T}_k is determined based on geometric considerations. The polar decomposition theorem is applied to compute the local corotating coordinate system. This method leads to a node-numbering-independent formulation and it passes the large-strain patch test (Crisfield, 1997).

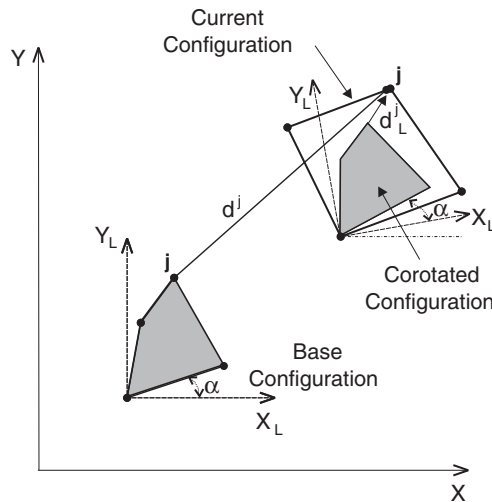


Fig. 1. Base and current configurations.

2.2. Nonlinear dynamics

It has been verified by Simo and Tarnow (1992), Simo et al. (1995), and by Crisfield et al. (1997), Crisfield and Shi (1994), Crisfield et al. (1996), and Galvanetto and Crisfield (1996) that the implicit dynamic algorithms often used in linear dynamics do not exhibit a good behaviour when applied to nonlinear dynamics. An approximately-energy-conserving-corotational algorithm, based on the mid-point rule, was proposed by Crisfield and Shi (1994) and it was shown that its application to beams provides stable and accurate solutions in the nonlinear regime.

The conventional implicit dynamic algorithms are characterized by determining the solution at time step $t + \Delta t$ using the solutions obtained at time step t . With the algorithm proposed by Crisfield and co-workers, the information obtained at the mid-steps $m_- = t - \Delta t/2$ and $m_+ = t + \Delta t/2$ is also used. Although this algorithm might appear more complex and more data has to be stored, the stability and accuracy obtained overcome these inconveniences as reported in the literature [e.g. Crisfield (1997)].

In a conventional implicit dynamic algorithm, the dynamic equation at time step $t + \Delta t$ is

$$\bar{\mathbf{g}}_{t+\Delta t} = \mathbf{f}_{it+\Delta t} - \mathbf{f}_{et+\Delta t} + \mathbf{M}\ddot{\mathbf{p}}_{t+\Delta t} = 0, \quad (4)$$

where $\bar{\mathbf{g}}_{t+\Delta t}$ is the dynamic out-of-balance force vector, $\mathbf{f}_{it+\Delta t}$ is the internal force vector at time instant $t + \Delta t$, $\mathbf{f}_{et+\Delta t}$ is the external force vector at time instant $t + \Delta t$, \mathbf{M} is the finite element mass matrix, and $\ddot{\mathbf{p}}_{t+\Delta t}$ is the nodal acceleration vector at time step $t + \Delta t$.

With the approximately energy conserving algorithm as originally proposed by Crisfield et al. (1996), Eq. (4) is rewritten at time step m_+ . The important step consists of determining the internal forces \mathbf{f}_{im_+} at the time interval mid-point, using the average of the initial and final time step internal forces. Note that the internal forces are not determined from the displacement at the time interval mid-point (Crisfield et al., 1997). The dynamic equations are written at the mid point as

$$\bar{\mathbf{g}}_{m_+} = \left(\frac{\mathbf{T}_t + \mathbf{T}_{t+\Delta t}}{2} \right)^T \frac{\mathbf{f}_{iLm_+}}{2} - \mathbf{f}_{em_+} + \mathbf{M} \left(\frac{\dot{\mathbf{p}}_{t+\Delta t} - \dot{\mathbf{p}}_t}{\Delta t} \right) = 0. \quad (5)$$

A predictor/corrector procedure is used. The predictor step consists of determining $\Delta \mathbf{p}$ from

$$\Delta \bar{\mathbf{q}}_e = \bar{\mathbf{K}}_{\mathbf{T},m_-} \Delta \mathbf{p}, \quad (6)$$

where

$$\bar{\mathbf{K}}_{\mathbf{T},m_-} = \mathbf{K}_{\mathbf{T},m_-} + \frac{2}{\Delta t^2} \mathbf{M}, \quad (7)$$

$$\Delta \bar{\mathbf{f}}_e = \mathbf{f}_{em_+} - \mathbf{f}_{im_-} + \frac{2}{\Delta t} \mathbf{M} \dot{\mathbf{p}}_t. \quad (8)$$

The matrix $\mathbf{K}_{\mathbf{T},m_-}$ is the nonlinear tangent stiffness matrix determined at time step m_- . The displacement at step $t + \Delta t$ is determined as

$$\mathbf{p}_{t+\Delta t} = \mathbf{p}_t + \Delta \mathbf{p}, \quad (9)$$

and the velocity is determined from

$$\dot{\mathbf{p}}_{t+\Delta t} = \frac{2}{\Delta t} \Delta \mathbf{p} - \dot{\mathbf{p}}_t. \quad (10)$$

As the solution does not satisfy the equilibrium, an iterative corrector step is applied until a convergence criterion is satisfied. Each iteration i consists of determining $\delta \mathbf{p}_{i+\Delta t}^i$ from

$$\bar{\mathbf{g}}_{m_+}^{i-1} + \bar{\mathbf{K}}_{\mathbf{T},m_+}^{i-1} \delta \mathbf{p}_{i+\Delta t}^i = 0, \quad (11)$$

where $\bar{\mathbf{g}}_{m_+}^{i-1}$ is determined applying $\dot{\mathbf{p}}_{t+\Delta t}^{i-1}$, \mathbf{f}_{iL}^{i-1} and $\mathbf{T}_{t+\Delta t}^{i-1}$ to Eq. (5). The element nonlinear tangent stiffness matrix $\bar{\mathbf{K}}_{m_+}$ is determined from

$$\begin{aligned} \delta \mathbf{f}_{im_+} &= \left(\frac{\mathbf{T}_t + \mathbf{T}_{t+\Delta t}}{2} \right)^T \delta \left(\frac{\mathbf{f}_{iL} + \mathbf{f}_{iL+\Delta t}}{2} \right) + \delta \left(\frac{\mathbf{T}_t + \mathbf{T}_{t+\Delta t}}{2} \right)^T \mathbf{f}_{iLm_+} \\ &= \left(\frac{\mathbf{T}_t + \mathbf{T}_{t+\Delta t}}{2} \right)^T \left(\frac{\delta \mathbf{f}_{iL+\Delta t}}{2} \right) + \left(\frac{\delta \mathbf{T}_{t+\Delta t}}{2} \right)^T \mathbf{f}_{iLm_+}, \end{aligned} \quad (12)$$

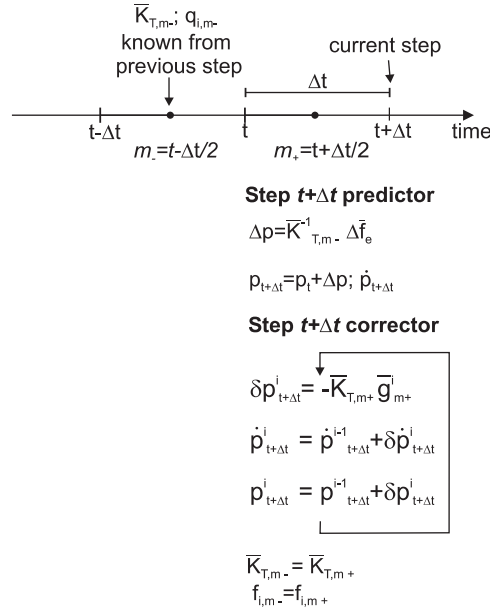


Fig. 2. Approximately-energy-conserving dynamic algorithm.

and thus the $\bar{\mathbf{K}}_{T,m+}$ matrix takes the form:

$$\bar{\mathbf{K}}_{T,m+} = \frac{1}{2} \left(\frac{\mathbf{T}_t + \mathbf{T}_{t+\Delta t}}{2} \right)^T \mathbf{K}_t \mathbf{T}_{t+\Delta t} + \mathbf{K}_{t\sigma}. \quad (13)$$

Note that for determining $\mathbf{K}_{t\sigma}$ one should use the internal force vector $\mathbf{f}_{i,m+}$. In each corrector iteration the displacement and velocity are updated. The velocity variation is determined from

$$\delta \dot{\mathbf{p}}_{t+\Delta t} = \frac{2}{\Delta t} \delta \mathbf{p}_{t+\Delta t}. \quad (14)$$

This procedure is illustrated in Fig. 2. It is noted that $\bar{\mathbf{K}}_{T,m-}$ and $\mathbf{f}_{i,m-}$ are known from the previous time step. In the predictor phase, $\Delta \mathbf{p}$ is calculated and the predicted $\mathbf{p}_{t+\Delta t}$ and $\dot{\mathbf{p}}_{t+\Delta t}$ are determined. The variables $\mathbf{p}_{t+\Delta t}^0$ and $\dot{\mathbf{p}}_{t+\Delta t}^0$ are set as $\mathbf{p}_{t+\Delta t}$ and $\dot{\mathbf{p}}_{t+\Delta t}$. In the corrector phase, the deformation variation $\delta \mathbf{p}_{t+\Delta t}^i$ is determined iteratively until a convergence criterion is satisfied. When that criterion is satisfied, $\bar{\mathbf{K}}_{T,m-}$ and $\mathbf{f}_{i,m-}$ are set as $\bar{\mathbf{K}}_{T,m+}$ and $\mathbf{f}_{i,m+}$ so they can be used in the next time step.

3. Fluid flow modelling

The fluid flow was modelled using the vortex-ring method which models inviscid, irrotational, and incompressible flows. This method is a simple way to obtain unsteady fluid flow solutions with just a two-dimensional grid, instead of a three-dimensional grid around the structure. At this stage, the goal was to evaluate the behaviour of the corotational approximately-energy-conserving algorithm within the staggered algorithm. Using a higher-order fluid model would induce extra complexities to the procedure. A code based on the Navier–Stokes equations would add difficulties as three-dimensional mesh generation, mesh deformation, and more computational time would be necessary.

The unsteady vortex-ring method is based on the concept of dividing the wing into panels and placing a vortex ring singularity element on each panel (Fig. 3). A linear algebraic equation system is formed from the Laplace equation and the zero normal flow boundary condition (Katz and Plotkin, 1991). The vortex strength is determined at each element, and from these values the aerodynamic forces on the structure are determined using the Kutta–Joukowski’s theorem.

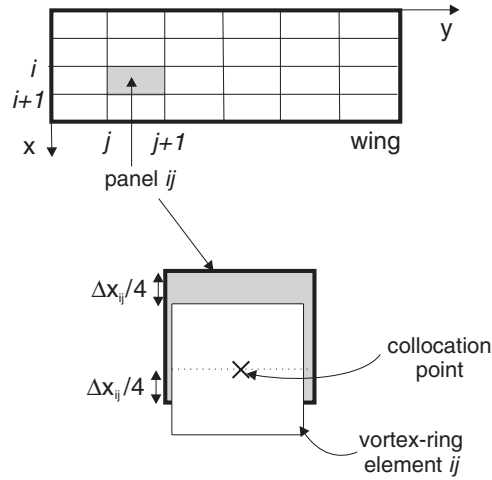


Fig. 3. Wing discretization.

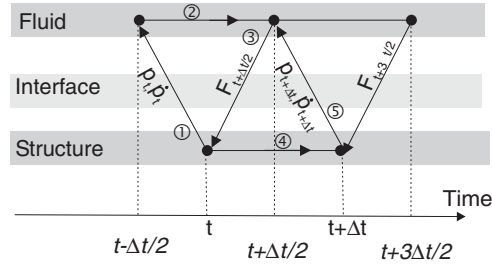


Fig. 4. Improved serial staggered algorithm.

4. Fluid–structure interaction

One of the most popular staggered algorithms applied to FSI (fluid–structure interaction) is the “serial conventional staggered” algorithm where the information between fluid and structure is transferred at time steps t , $t + \Delta t$, $t + 2\Delta t$, etc. The algorithm used in this study is slightly different; it was proposed by Farhat and Lesoinne (2000) and it was named as the “improved serial staggered” procedure (ISS). The structural deformation transferred to the fluid is determined with the structural code at time steps t , $t + \Delta t$, etc. whereas the loads on the structure are determined with the fluid code at time steps $t - \Delta t/2$, $t + \Delta t/2$, etc. (Fig. 4). Although this might seem more complex, it was proved to be more accurate and efficient, allowing for larger time steps.

Knowing the structure initial deformation \mathbf{p}_0 and velocity $\dot{\mathbf{p}}_0$, the algorithm starts by initializing the fluid dynamic mesh motion on the structure surface at time $(-\Delta t/2)$ with

$$\mathbf{x}_{-\Delta t/2} = \mathbf{p}_0 - \frac{\Delta t}{2} \dot{\mathbf{p}}_0. \quad (15)$$

Next, the flow problem is solved and the pressure field at time $t + \Delta t/2$ is determined and converted to the nodal structural loads $\mathbf{F}_{t+\Delta t/2}$. The structural displacement $\mathbf{p}_{t+\Delta t}$ and the velocity $\dot{\mathbf{p}}_{t+\Delta t}$ due to these loads are determined solving the finite element dynamic equations. Next, the fluid mesh is deformed using

$$\mathbf{x}_{t+\frac{1}{2}\Delta t} = \mathbf{x}_{t-\frac{1}{2}\Delta t} + \Delta t \dot{\mathbf{p}}_t. \quad (16)$$

The fluid flow solution is determined and this procedure is successively repeated.

5. Numerical results

5.1. Nonlinear structures

To show the validity of the structural code developed, the approximately-energy-conserving corotational algorithm was applied to two nonlinear structural dynamic problems. The results obtained are presented next.

5.1.1. Square plate subjected to a uniform pressure

The dynamic nonlinear analysis of a simply supported square plate, illustrated in Fig. 5, subjected to an impulsive uniform pressure was performed using the approximately-energy-conserving corotational algorithm. The results obtained were compared with the numerical ones obtained by Belytschko et al. (1984) and the analytical solution obtained by Balmer and Witmer (1964).

The plate center-point vertical displacement obtained is presented in Fig. 6. Only a quarter of the plate was modelled due to the load and geometry symmetry. The problem was solved with a 6×6 mesh and a $\Delta t = 4 \times 10^{-5}$ s time step.

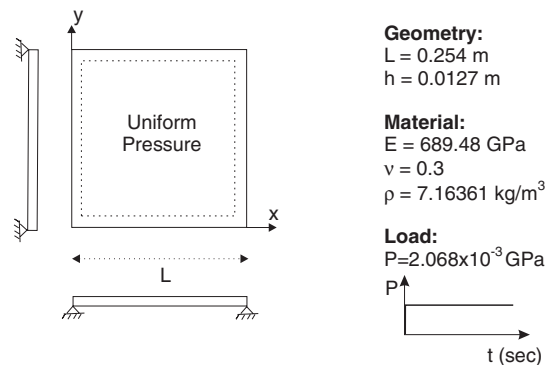


Fig. 5. Square plate under impulsively uniform pressure.

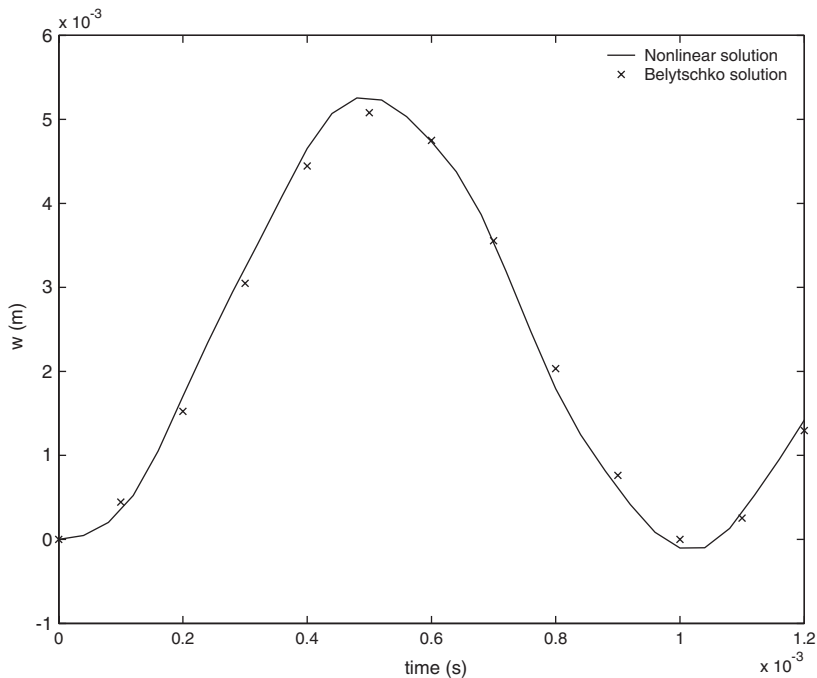


Fig. 6. Simply supported square plate center point out-of-plane deformation.

Table 1
Simply supported square plate results

Solution	Time step	No. of elements	Max. w (cm)
Present solution	4×10^{-5}	36	0.5326
Analytical (Balmer and Witmer, 1964)	None	None	0.5408
Triangular elements (Belytschko et al., 1984)	4×10^{-6}	32	0.5070
Quadrilateral elements (Belytschko et al., 1984)	6×10^{-6}	16	0.5083

The solution obtained in the literature (Belytschko et al., 1984) is based on an explicit algorithm with a corotational description to treat the geometric nonlinearities. They used triangular and quadrilateral elements.

The results obtained with the present theory agree quite well with the literature. Table 1 presents the different solutions. The literature solutions (Belytschko et al., 1984) were obtained with smaller time steps because an explicit solution procedure was used. The present solution is closer to the analytical solution (Balmer and Witmer, 1964) than the explicit finite element solution (Belytschko et al., 1984).

This problem was also solved with the Newmark method (trapezoidal rule), so its stability could be compared with the approximately-energy-conserving corotational algorithm. Results were obtained for a longer simulation time, in order to, observe the algorithms stability behavior. Vertical displacement and the total energy variations are presented in Fig. 7.

As can be observed, the solutions do not differ, but the energy change variation obtained with the Newmark method is more pronounced. For the range of simulation, this energy variation did not affect the stability or accuracy, which proves that for certain kind of problems the nonlinear Newmark method delivers good solutions.

5.1.2. Beam-like-plate subjected to a point load

Fig. 8 illustrates the experimental setup and data presented by Berggren (2001). Clamped boundary conditions are applied. The beam is initially straight.

The total force results from the gravity and the applied force on the plate. The applied force depends on the point P_0 displacement and it is determined as

$$\mathbf{F}_s(t) = \mathbf{F}_s \frac{\mathbf{P}_f - (\mathbf{P}_0 + \mathbf{u}_0(t))}{\|\mathbf{P}_f - (\mathbf{P}_0 + \mathbf{u}_0(t))\|}, \quad (17)$$

where \mathbf{u}_0 is point P_0 displacement determined with the finite element procedure, \mathbf{P}_f is point P_f position vector and \mathbf{P}_0 is point P_0 position vector. Dynamic experimental results were obtained starting from the static solution with $F_s = 10$ N and suddenly the load was removed. The numerical results were obtained setting the initial velocity to zero and the initial displacement to the displacement obtained from the static nonlinear solution with $F_s = 10$ N.

Two different methods were used to determine the dynamic nonlinear solution: the corotational approximately-energy-conserving method and the implicit Newmark method (trapezoidal rule). Both methods used the same 2×10 mesh and a $\Delta t = 0.002$ s time step. In Fig. 9, the numerical results obtained with the present method and experimental results obtained by Berggren (2001) are presented. The graphic presents the point P_0 displacements u, v, w in the x, y, z directions, respectively. The curves have the same kind of behaviour. As damping was not taken into account during the numerical simulation, it is observed that the amplitude of the numerical results does not decrease with time. Also, it can be observed that the damping induces a lower frequency. In Fig. 10 it is possible to compare these results with the ones obtained with the Newmark method. The energy variation of both methods is also presented. Initially, both algorithms generate identical results. However, before the 1 s mark, the Newmark method energy is not preserved and the algorithm fails.

With these examples the accuracy and stability properties are studied of the corotational approximately-energy-conserving algorithm with a four-node flat element. Obtaining stable structural solutions for a long time period is very important during aeroelastic computations, particularly to analyze the deformation curves and to interpret the aeroelastic behaviour.

5.2. Nonlinear aeroelastic results

As an illustration of the developed method, consider the stability determination of a cantilevered wing vibration. The fluid flow influences the wing oscillatory behaviour which might be damped, diverging, or the amplitude might not

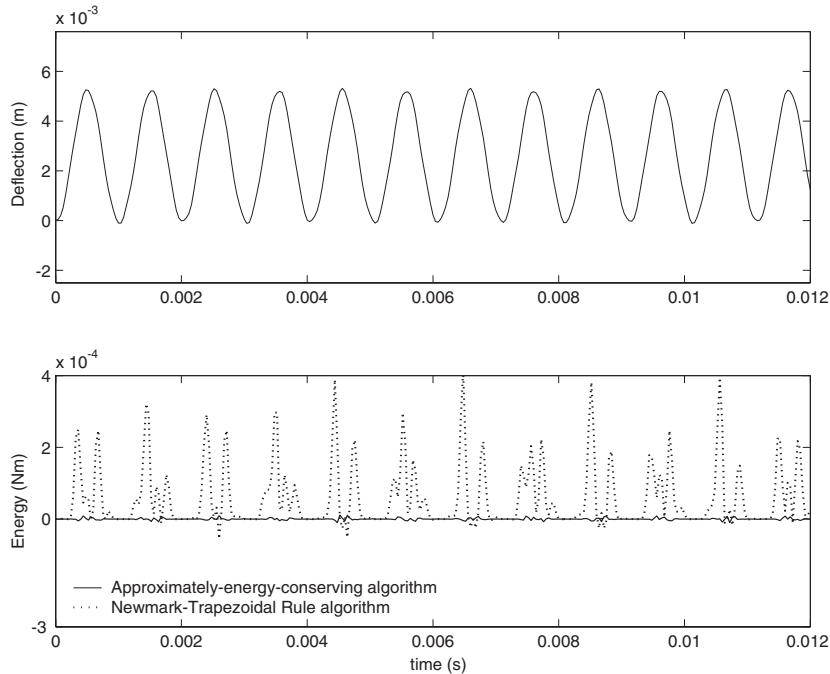


Fig. 7. Square plate results: Newmark algorithm and proposed algorithm.

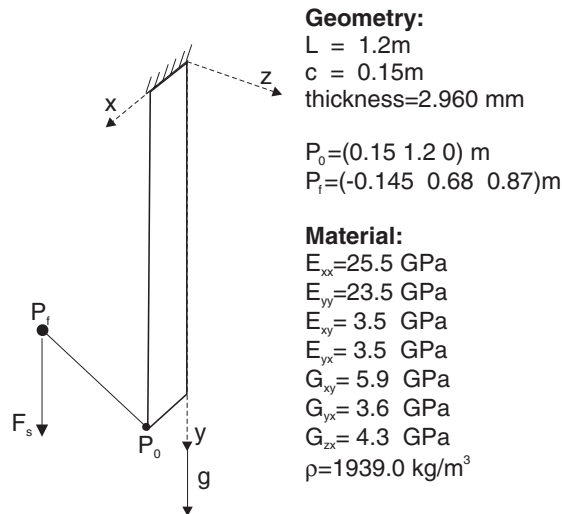


Fig. 8. Cantilever beam problem.

change. Depending on the type of motion, the wing might be stable, unstable or neutrally stable. The simulation starts by determining the structural natural frequencies and respective vibration modes. Then, the wing is deformed into the shape of one or more modes and the initial velocity is set to zero, or conversely, it has a nonzero initial vibration velocity and no deformation. After the fluid steady state solution is determined, the calculated static aerodynamic loads are applied to the wing and the finite element structural equations are solved to determine the structural deformation due to the aerodynamic loads. After, a mode decomposition is performed using the least-squares method (Bennet and Desmarais, 1975). A time-dependent displacement solution is obtained and the dynamic response is either damped, diverging or it displays neutrally stable vibrations. As the fluid and structure grids do not coincide, an interpolation/extrapolation procedure must be used to transfer data from one field to the other. As the present studied aeroelastic

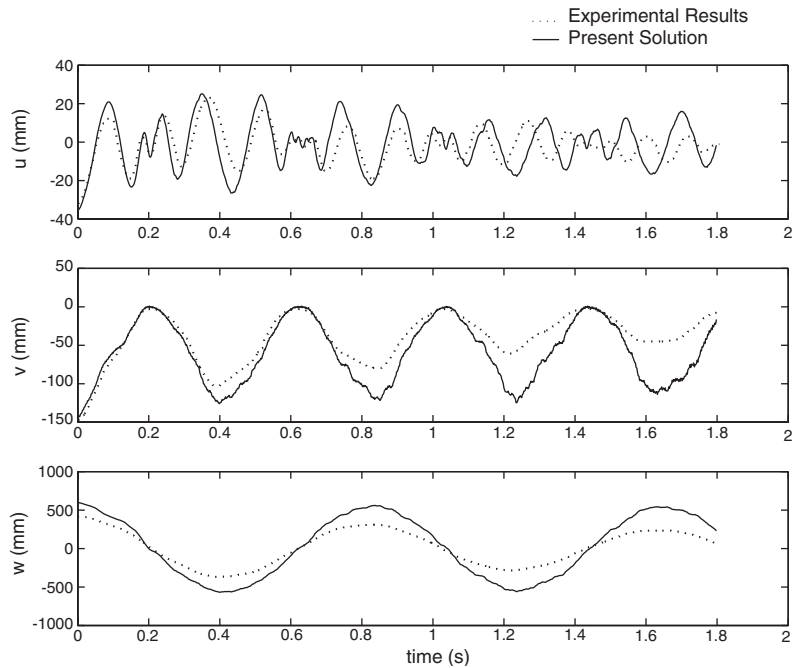


Fig. 9. Cantilever beam numerical and experimental results.

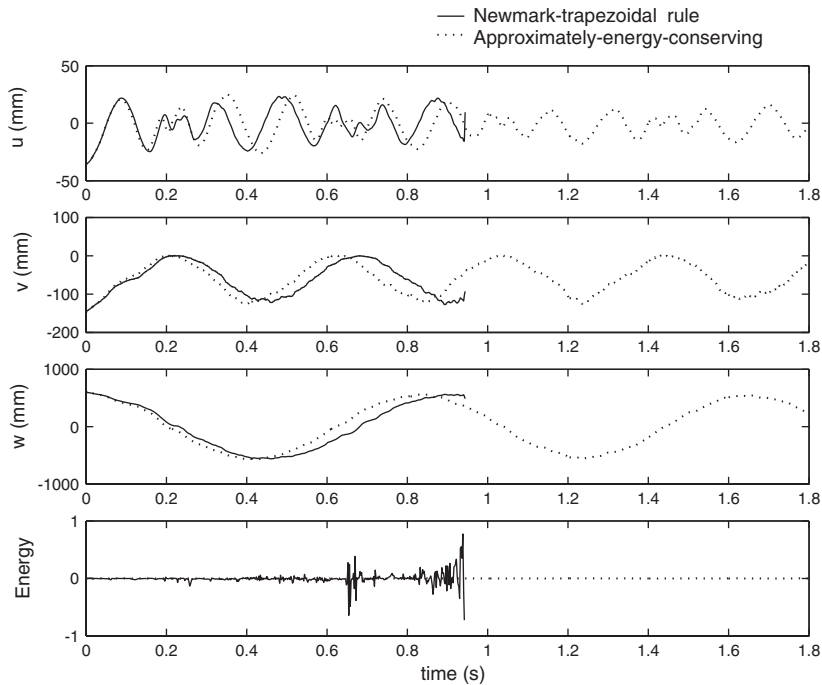


Fig. 10. Cantilever beam results: Newmark method vs. proposed method.

problem has a simple geometry, the infinite plate spline (IPS) method proposed by [Harder and Desmarais \(1972\)](#) is used.

An aluminium square plate subjected to airflow with a low speed V_T was studied ([Fig. 11](#)). The structure was modelled using an 8×8 grid. The fluid solution was obtained using 13 panels in the x -direction and 30 in the

y -direction. A convergence study was performed to determine the optimal number of elements. The time step was defined as $\Delta t = \Delta X / V_T$, where ΔX is the fluid panel length in the x direction. The angle of attack is zero. This problem was studied by Tang et al. (1999a) using a vortex-lattice aerodynamic method and a nonlinear structural modal analysis.

To validate the staggered algorithm code, the problem was solved assuming a linear structure. Thus, the implicit Newmark method (trapezoidal rule) was used to obtain the linear dynamic structural solution. First, the natural modes and frequencies were determined. The first four natural frequencies were $f_1 = 2.99$ Hz, $f_2 = 7.28$ Hz, $f_3 = 19.05$ Hz and $f_4 = 24.27$ Hz. The plate was initially deformed with each one natural vibration mode shape. Then the fluid flow equations and the structural finite element equations were solved in time. It was observed that, for low flow speeds, the plate kept vibrating with the respective excited natural frequency and it displayed a decaying oscillatory motion. Fig. 12 presents the tip displacement obtained exciting the second vibration mode for $V_T = 10$ m/s.

As the flow speed increased, mode coupling was observed. At the speed of $V_T = 42$ m/s the first (bending) and second (torsion) modes coupled and the plate damping was approximately zero. Fig. 13 presents point $x = 0.75c$ and

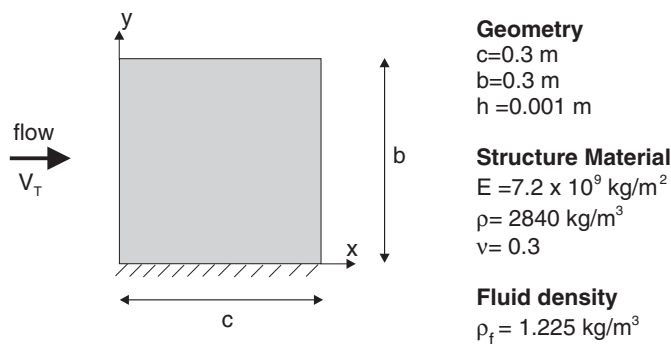


Fig. 11. Aeroelastic problem studied.

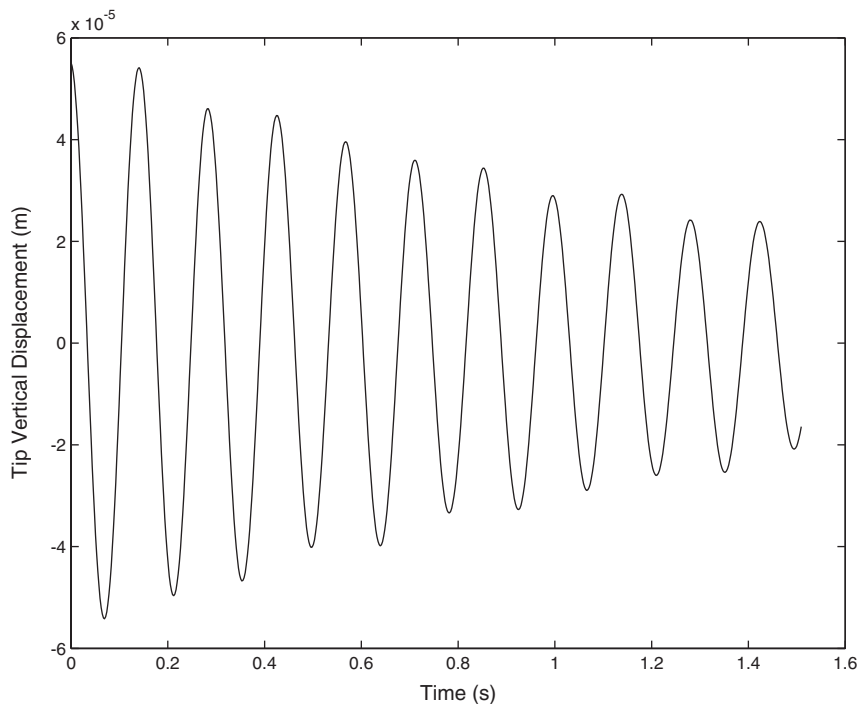


Fig. 12. Tip out-of-plane displacement for $V_T = 10$ m/s.

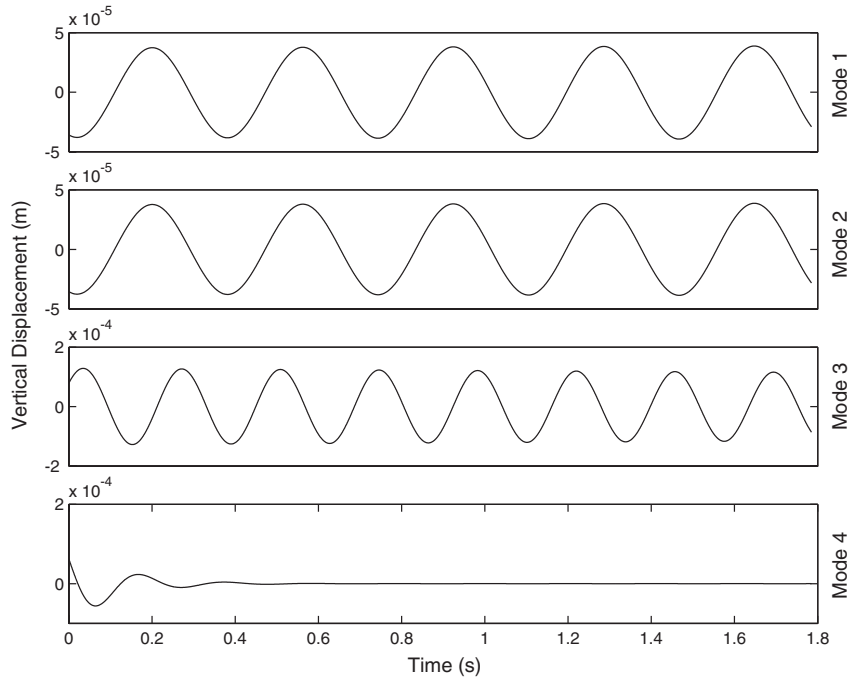


Fig. 13. Out-of-plane displacement mode decomposition for $V_T = 42$ m/s.

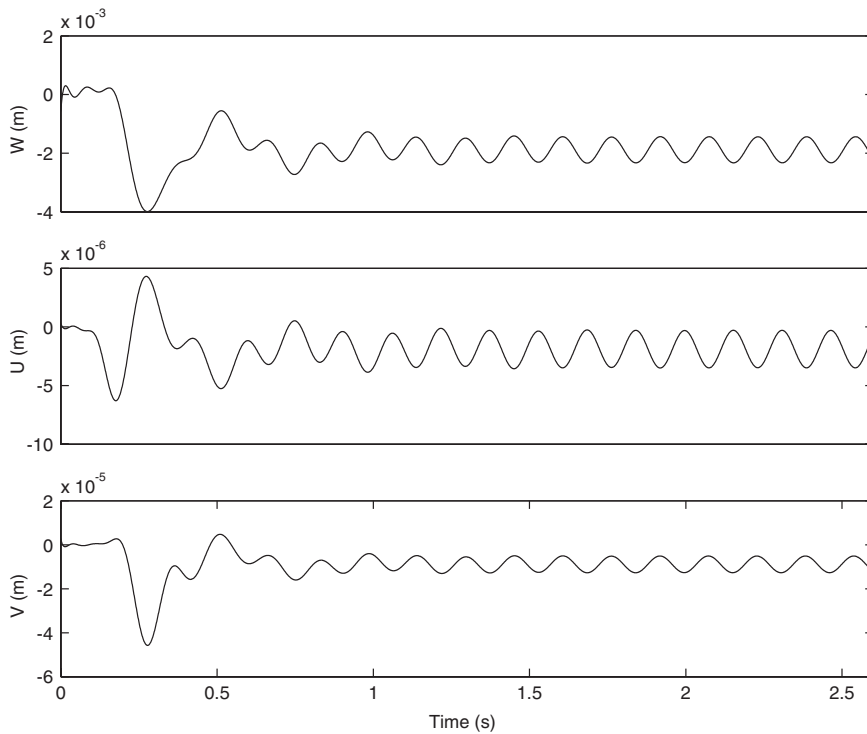


Fig. 14. Nonlinear plate deformations for $V_T = 44$ m/s.

$y = 0.75b$ out-of-plane displacement for $V_T = 42$ m/s. These curves are the mode decomposition result of the time curve obtained with the FSI algorithm.

This is the point from which the linear theory predicts that a decaying oscillatory motion becomes a growing oscillatory motion. This value of flutter speed agrees with the literature (Tang et al., 1999a), thus validating the

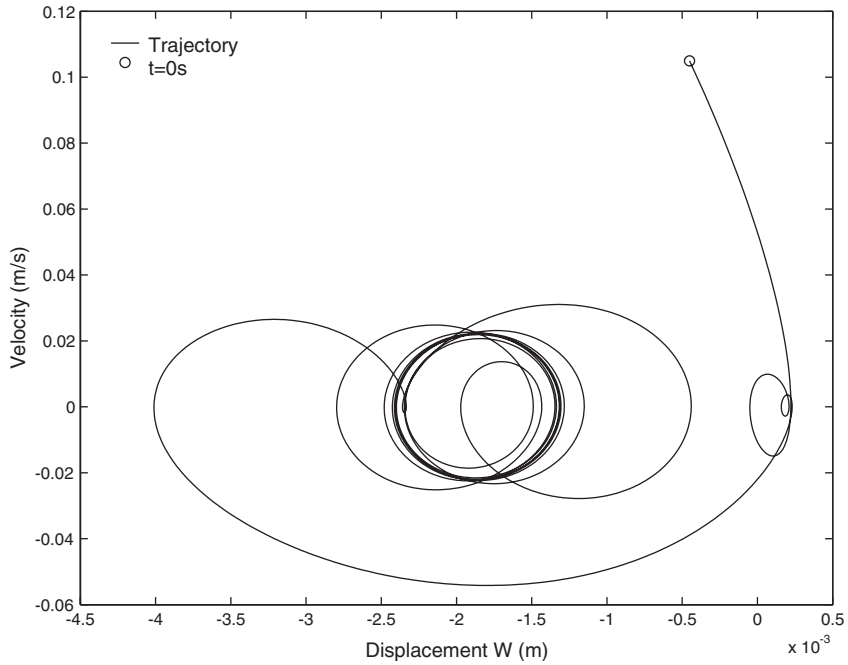


Fig. 15. Deformation W phase portrait for $V_T = 44$ m/s.

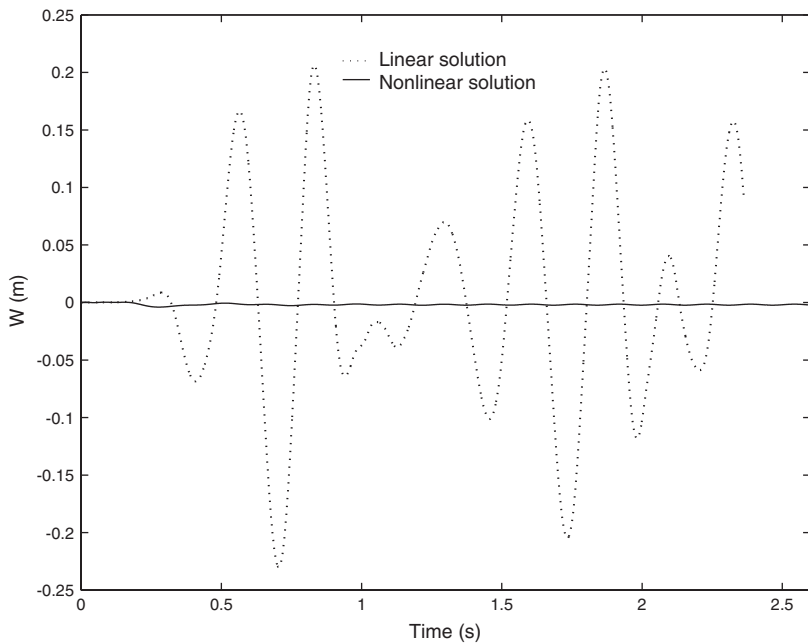


Fig. 16. Linear and nonlinear response for $V_T = 44$ m/s.

staggered procedure. Besides, preliminary wind tunnel tests were performed and it was observed a substantial oscillatory motion in this velocity range.

Next, the same problem was studied assuming a nonlinear structure. Time deformation results were obtained for velocities greater than the flutter speed. When using the linear structural theory, the in-plane deformation u and v were

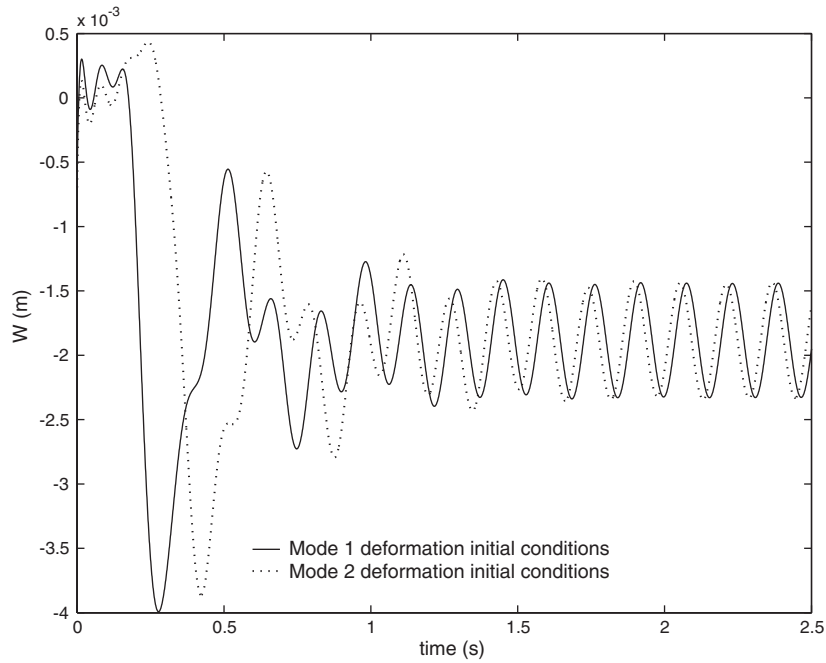


Fig. 17. Initial deformation influence on nonlinear response for $V_T = 44$ m/s.

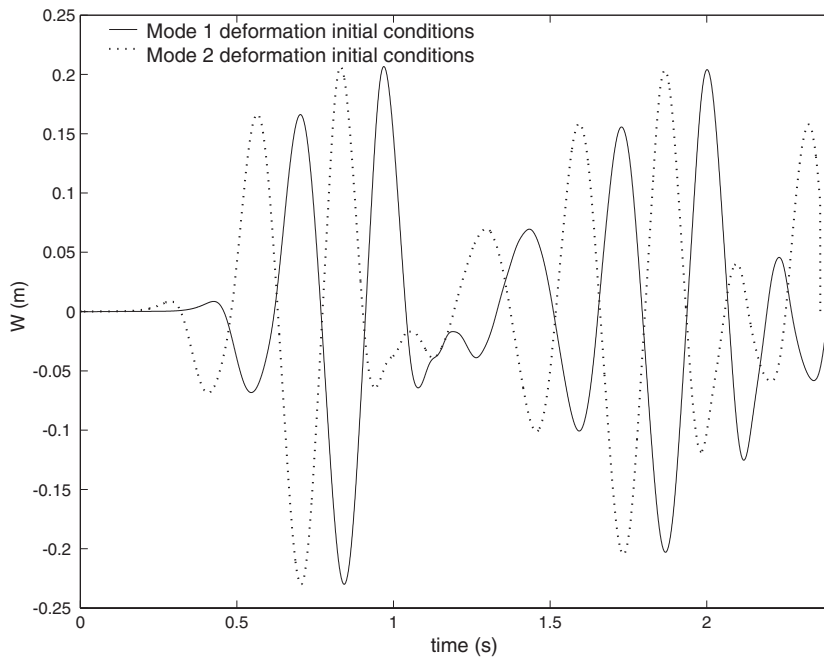


Fig. 18. Initial deformation influence on linear response for $V_T = 44$ m/s.

neglected. Now, with the nonlinear structural theory, these deformations become important. Although they are smaller than the out-of-plane deformations, they exhibit interesting dynamic characteristics. Fig. 14 represents the in-plane (u, v) and out-of-plane (w) deformation variation with time at the point $x = 0.5c$ and $y = 0.75b$ for $V_T = 44$ m/s. It is observed that the nonlinear dynamic response settles to a steady state sinusoidal motion after 1 s, indicating LCO behaviour. The LCO phenomenon is also observed in the phase portrait obtained (Fig. 15). The trajectory seems initially chaotic but it converges to a closed trajectory. This is characteristic of the limit cycle oscillation phenomenon.

Fig. 16 presents the results obtained with the linear and the nonlinear structural theory. The linear theory predicted the occurrence of flutter, while the nonlinear theory predicted limit cycle oscillations. As observed in Fig. 16, during the first 0.1 s the linear and nonlinear solutions apparently seem to indicate similar behaviour. However, the linear deformation keeps growing, while the nonlinear deformation oscillates with smaller amplitude. The difference between the two solutions is due to the nonlinear coupling between membrane and bending stresses in the plate. During the first few instants, the deformations u and v are very small. As the vertical deformation w grows, the nonlinear effects become more accentuated and the coupling between bending and membrane stresses increases. The deformations u and v start presenting a small oscillatory motion. From the energy point of view, in the linear case the fluid energy is transferred to the structure and it manifests itself as an increase in the out-of-plane deformation. At the onset of flutter, the energy transferred is greater than the structural potential energy, and the structural response diverges. In the nonlinear case, this energy is distributed also to the in-plane deformations, thus dividing the total energy into three directions and not being able to create instability in any particular displacement mode.

In short, when using the linear theory an oscillatory growing motion is observed. When using the nonlinear theory, an oscillatory sustained motion with smaller amplitude is found (LCO). The out-of-plane displacement presents an oscillatory motion in the negative direction. This fact was observed during wind tunnel tests.

To show that the results do not depend on the structural initial deformation, simulations were performed with initial excitation of other structural modes. Figs. 17 and 18 represent the results obtained deforming the structure with the shape of the first and second natural modes. As can be observed, the out-of-plane deformation shows the same kind of behaviour and, as time progresses, the nonlinear solutions tend to coincide defining a limit cycle oscillation.

6. Conclusions

The development and application of nonlinear fluid–structure interaction tools to study aeroelastic problems has been presented. The linear structural theories do not properly account for the effect of large structural deformations in high aspect ratio wings. To this end, it has been shown that when considering nonlinear structural effects leads to limit cycle oscillations rather than the unstable behaviour predicted by the linear solution.

The corotational finite element method using the approximately-energy-conserving algorithm to model geometrically nonlinear structures and based on existing linear finite element codes was presented. The nonlinear structural solver was coupled with a fluid solver using an improved serial staggered algorithm.

Two geometrically nonlinear structural dynamic problems were studied using the proposed algorithms combined with the conventional implicit nonlinear Newmark method. The results demonstrate that the proposed algorithms for solving nonlinear fluid–structure interaction problems are accurate and stable. The numerical results agree with the case studies reported in the literature.

Acknowledgements

This research was supported by the Fundação para a Ciência e Tecnologia in the framework of the Ph.D. Scholarship SFRH/BD/2786, the POCTI/EME/38016/2001 project and the RTO-NATO Applied Vehicle Technology Panel Support Program Project P126.

References

- Alonso, J., Jameson, A., 1994. Fully-implicit time-marching aeroelastic solutions. AIAA Paper 94-0056.
- Alonso, J., Martinelli, L., Jameson, A., 1995. Multigrid unsteady Navier–Stokes calculations with aeroelastic applications. AIAA Paper 94-0048.

- Balmer, H., Witmer, E., 1964. Theoretical-experimental correlation of large dynamic and permanent deformation of impulsively loaded simple structures. Technical Report FDP-TDR-64-108, Air Force Dynamics Laboratory, Wright Patterson AFB, OH, USA.
- Belytschko, T., Lin, J., Tsay, C.-S., 1984. Explicit algorithms for the nonlinear dynamics of shells. *Computer Methods in Applied Mechanics and Engineering* 42, 225–251.
- Bennet, R., Desmarais, R., 1975. Curve fitting of aeroelastic transient response data with exponential functions, Flutter testing techniques. NASA SP-415, pp. 43–58.
- Berggren, D., 2001. Experimental validation of nonlinear shell structural dynamics. *AIAA Journal* 39 (9), 1825–1827.
- Crisfield, M., 1990. A consistent co-rotational formulation for non-linear, three-dimensional, beam-elements. *Computer Methods in Applied Mechanics and Engineering* 81, 131–150.
- Crisfield, M., 1997. *Non-linear Finite Element Analysis of Solids and Structures—Advanced Topics*, vol. 2. Wiley, New York.
- Crisfield, M., Moita, G., 1996. A unified co-rotational framework for solids, shells and beams. *International Journal of Solids and Structures* 33 (20–22), 2969–2992.
- Crisfield, M., Shi, J., 1994. A co-rotational element/time-integration strategy for non-linear dynamics. *International Journal for Numerical Methods in Engineering* 37, 1897–1913.
- Crisfield, M., Moita, G., Jelenic, G., Lyons, L., 1995. Enhanced lower-order element formulations for large strains. *Computational Mechanics* 17, 62–73.
- Crisfield, M., Jelenic, G., Zhong, H.-G., Fan, Z., 1996. Static and dynamic non-linear analysis of structures. *Computational Methods in Applied Sciences*, 9–21.
- Crisfield, M., Jelenic, G., Mi, Y., Zhong, H.-G., Fan, Z., 1997. Some aspects of the non-linear finite element method. *Finite Element Analysis and Design* 27, 19–40.
- Dowell, E., 1966. Nonlinear oscillations of a fluttering plate. *AIAA Journal* 4 (7), 1207–1275.
- Dowell, E.H., 1967. Nonlinear oscillations of a fluttering plate II. *AIAA Journal* 5 (10), 1856–1862.
- Dowell, E.H., 1969. Nonlinear flutter of curved plates. *AIAA Journal* 7 (3), 424–431.
- Dowell, E.H., 1970. Nonlinear flutter of curved plates II. *AIAA Journal* 8 (2), 259–261.
- Farhat, C., Lesoinne, M., 1998. Fast staggered algorithms for the solution of three-dimensional nonlinear aeroelastic problems. AGARD Report R-822, Numerical unsteady aerodynamic and aeroelastic simulation, NATO.
- Farhat, C., Lesoinne, M., 2000. Two efficient staggered algorithms for the serial and parallel solution of the three-dimensional nonlinear transient aeroelastic problems. *Computer Methods in Applied Mechanics and Engineering* 182, 499–515.
- Farhat, C., Pierson, K., Degand, C., 2001. Multidisciplinary simulation of the maneuvering of an aircraft. *Engineering with Computers* 17 (1), 16–27.
- Felippa, C., Park, K., 1980. Staggered transient analysis procedures for coupled mechanical systems: formulation. *Computer Methods in Applied Mechanics and Engineering* 24, 61–111.
- Galvanetto, U., Crisfield, M., 1996. An energy-conserving co-rotational procedure for the dynamics of planar beam structures. *International Journal for Numerical Methods in Engineering* 39, 2265–2282.
- Garcia, J. A., Guruswamy, G., 1999. Aeroelastic analysis of transonic wings using Navier–Stokes equations and a nonlinear beam finite element method. *AIAA Paper* 99-1215.
- Harder, R., Desmarais, R., 1972. Interpolation using surface splines. *Journal of Aircraft* 9 (2), 189–191.
- Hodges, D., 1990. A mixed variational formulation based on exact intrinsic equations for dynamics of moving beams. *International Journal of Solid Structures* 26 (11), 1253–1273.
- Kamakoti, R., Lian, Y., Regisford, S., Kurdila, A., Shyy, W., 2002. Computational aeroelasticity using a pressure-based solver. *AIAA Paper* 2002-0869.
- Katz, J., Plotkin, A., 1991. *Low-Speed Aerodynamics—From Wing Theory to Panel Methods*. McGraw-Hill series in Aeronautical and Aerospace Engineering. McGraw-Hill, New York.
- Lee-Raush, E., Batina, J., 1993. Calculation of agard wing 445.6 flutter using Navier–Stokes aerodynamics. *AIAA Paper* 93-3476.
- Liu, F., Cai, J., Zhu, Y., Wong, A., Tsai, H., 2000. Calculation of wing flutter by a coupled CFD-CSD method. In: *Proceedings of the 38th Aerospace Sciences Meeting and Exhibit*, Reno, NV, USA.
- Liu, F., Cai, J., Zhu, Y., 2001. Calculation of wing flutter by coupled fluid–structure method. *Journal of Aircraft* 38 (2), 334–342.
- Moita, G. F., 1994. Non-linear finite element analysis of continua with emphasis on hyperelasticity. Ph.D. thesis, University of London, UK.
- Moita, G., Crisfield, M., 1996. A finite element formulation for 3-D continua using the co-rotational technique. *International Journal for Numerical Methods in Engineering* 39, 3775–3792.
- Park, K., Felippa, C., 1980. Partitioned transient analysis procedures for coupled-field problems: accuracy analysis. *Journal of Applied Mechanics* 47, 919–926.
- Park, K., Felippa, C., DeRuntz, J., 1977. Stabilization of staggered solution procedures for fluid–structure interaction analysis. *Computational methods for fluid–structure interaction problems*; ASME Applied Mechanics Symposia Series, AMD-vol. 26.
- Patil, M., 1999. Nonlinear aeroelastic analysis, flight dynamics and control of a complete aircraft. Ph.D. thesis, Georgia Institute of Technology, USA.
- Patil, M., Hodges, D., 1998. Nonlinear aeroelasticity and flight dynamics of aircraft in subsonic flow. In: *Proceedings of the 21st Congress of International Council of the Aeronautical Sciences*, Melbourne, Australia.
- Patil, M., Hodges, D., Cesnik, C., 1998. Nonlinear aeroelastic analysis of aircraft with high-aspect-ratio wings. *AIAA Paper* 98-1955.

- Patil, M., Hodges, D., Cesnik, C., 1999. Characterizing the effects of nonlinearities on aeroelastic behavior of high-aspect-ratio wings. Presented at the International Forum on Aeroelasticity and Structural Dynamics, Williamsburg, Virginia, USA.
- Patil, M., Hodges, D., Cesnik, C., 2001. Limit cycle oscillations in high-aspect-ratio wings. *Journal of Fluids and Structures* 15, 107–132.
- Peng, X., Crisfield, M., 1992. A consistent co-rotational formulation for shells using triangular elements with constant strain and constant curvature. *International Journal for Numerical Methods in Engineering* 35, 1829–1847.
- Piperno, S., Farhat, C., Lorrouturou, B., 1995. Partitioned procedures for the transient solution of coupled aeroelastic problems. *Computer Methods in Applied Mechanics and Engineering* 124, 79–112.
- Rankin, C., Brogan, F., 1986. An element independent corotational procedure for the treatment of large rotations. *ASME Journal of Pressure Vessel Technology* 108, 165–174.
- Relvas, A., 2002. Computational fluid–structure interaction modelling of non-linear aeroelastic structures. Master’s Thesis, Department of Mechanical Engineering, University of Victoria, Canada.
- Simo, J., Tarnow, N., 1992. The discrete energy-momentum method. Conserving algorithms for nonlinear elastodynamics. *Zeitschrift für angewandte Mechanik und Physik* 43, 757–792.
- Simo, J., Tarnow, N., Doblare, M., 1995. Non-linear dynamics of three-dimensional rods: exact energy and momentum conserving algorithms. *International Journal for Numerical Methods in Engineering* 38, 1431–1473.
- Tang, D., Conner, M., Dowell, E., 1998. Reduced-order aerodynamic model and its application to a nonlinear aeroelastic system. *Journal of Aircraft* 35 (2), 332–338.
- Tang, D., Dowell, E., Hall, K., 1999a. Limit cycle oscillations of a cantilevered wing in low subsonic flow. *AIAA Journal* 37 (3), 364–371.
- Tang, D., Henry, J., Dowell, E., 1999b. Limit cycle oscillation of delta wing models in low subsonic flow. *AIAA Journal* 37 (11), 1355–1362.
- Weiliang, Y., Dowell, E., 1991. Limit cycle oscillation of a fluttering cantilever plate. *AIAA Journal* 29 (11), 1929–1936.